Quantifying uncertainties in Atmospheric Infrared Sounder (AIRS) spatial response functions

Igor Yanovsky[a], Thomas S. Pagano[a], Evan M. Manning[a], Steven E. Broberg[a], and Brian M. Sutin[b]

[a]Jet Propulsion Laboratory, California Institute of Technology, Pasadena, CA, USA
[b]Skewray Research, LLC, South Pasadena, CA, USA

ABSTRACT

Quantifying uncertainties in Atmospheric Infrared Sounder (AIRS) spatial response functions (SpatialRFs) is critical for enhancing the quality of climate data records. Previously, AIRS in-flight SpatialRF calibrations have utilized an incomplete set of pre-flight data obtained during instrument assembly. In our current work, we combined various pre-flight data sets to interpolate a complete set of pre-flight SpatialRFs. Concurrently, we employed two consecutive days of AIRS and Moderate Resolution Imaging Spectroradiometer (MODIS) data to independently retrieve in-flight SpatialRFs for multiple channels and scan angles. Our methodology, based on our previous work, aligns AIRS and MODIS radiances to derive spatially corrected SpatialRFs. This paper compares in-flight SpatialRFs obtained from consecutive days and examines the discrepancies between pre-flight SpatialRFs from a completed set and in-flight SpatialRFs. Employing the total variation distance metric with two days of consecutive data revealed that the average uncertainties in in-flight SpatialRFs are approximately 5%, attributed mainly to noise, which establishes a baseline. In contrast, pre-flight SpatialRFs displayed an average uncertainty of about 16% when compared to the values derived in-flight. Our findings underscore the value of reconstruction techniques to derive in-flight SpatialRFs to validate pre-flight measurements, which is vital for ensuring the long-term reliability and precision of climate data records obtained from AIRS.

Keywords: Atmospheric Infrared Sounder (AIRS), Spatial Response Function, Point Spread Function (PSF), Uncertainty Quantification, Instrument Calibration

1. INTRODUCTION

Launched on the EOS Aqua spacecraft on May 4, 2002, the Atmospheric Infrared Sounder (AIRS) has been instrumental in advancing climate research and enhancing weather prediction by collecting critical water vapor and temperature measurements.[1–6] AIRS utilizes 2378 infrared channels that capture radiances across wavelengths ranging from 3.7 µm to 15.4 µm. As a whisk broom sensor, it conducts scans at 90 different angles across the satellite's path, covering the entire globe daily with a spatial resolution of 13.5 km.

From the Aqua orbit altitude of 705 km, the projected beam is nominally 1.1 degrees as measured from the satellite. The beam shape, or Spatial Response Function (SpatialRF), is irregular and depends on the cross-track scan angle, varying from channel to channel. Most channels exhibit similar SpatialRFs; however, due to the nature of the AIRS design, the SpatialRFs can change substantially for channels near the end of the 17 individual detector modules. SpatialRFs represent the response of each individual channel to the underlying scene radiance. The signal from the AIRS is proportional to the product of the underlying radiance distribution of the scene and the SpatialRF.

Most AIRS channels have two redundant detectors, which can have distinct SpatialRFs. In most cases the signals are combined in the instrument, downlinking a combined "AB" measurement. When one of the redundant detectors is of low quality, A-only or B-only measurements are made.

Further author information: (Send correspondence to I.Y.)
I.Y.: E-mail: Igor.Yanovsky@jpl.nasa.gov, T.S.P.: E-mail: Thomas.S.Pagano@jpl.nasa.gov,
E.M.M.: E-mail: Evan.M.Manning@jpl.nasa.gov, S.E.B: E-mail: Steven.E.Broberg@jpl.nasa.gov,
B.M.S: E-mail: spie3@skewray.com

The Moderate Resolution Imaging Spectroradiometer (MODIS), also launched on the EOS Aqua satellite, complements AIRS with its 36 channels that record radiances in wavelengths from 0.4 µm to 14.4 µm. MODIS offers varied spatial resolutions—1 km, 500 m, and 250 m—and conducts ten scans per scan at each 1 km channel resolution, mirroring AIRS in scanning across the satellite's trajectory.[7] Our focus is on MODIS's 11 µm channel 31, a window channel with low water vapor absorption, which aids in understanding the in-flight variations of AIRS's spatial response functions. Previous studies have demonstrated that enhancing the spatial response functions of AIRS can significantly improve the intercomparison of radiances with MODIS, particularly in non-uniform scenes.[8]

2. SPATIAL PERFORMANCE CHARACTERIZATION OF THE AIRS INSTRUMENT

The spatial performance of the Atmospheric Infrared Sounder (AIRS) is defined by several key parameters.[9] These include the instantaneous field of view (IFOV) diameter, the infrared (IR) boresight's orientation relative to reference flats on the AIRS base, spatial uniformity across different wavelengths (Cij), and the synchronization of detector integrations with wavelength given AIRS's scanning capability, along with the limits of the out-of-field of view response.

Spatial response characterization was primarily conducted at the level of the IR Sensor Assembly rather than the complete instrument. Nevertheless, sufficient testing on the fully assembled instrument confirmed the accuracy of earlier data. Initial data collection involved detailed 2D raster map scans to assess instrument response, whereas later tests only required vertical and horizontal cross-axis spatial scans through the AIRS IFOV center. These cross-axis scans were compared to similar tests from the IR Sensor Assembly, showing a high degree of similarity in response contours for spectral samples near the center of the shortest wavelength array.[9] This consistency across a full range of wavelengths confirmed that full raster scanning in two dimensions was unnecessary for the instrument. The comprehensive scans from the IR Sensor Assembly stage were deemed representative of the entire AIRS instrument.

IFOV diameters for all spectral samples were calculated from the IR Sensor Assembly measurements, adhering to the requirement that they not exceed 1.1°. It was observed that the IFOVs were slightly elliptical, approximately 5%, with diameters determined by the geometric mean of the major and minor ellipse axes. This specification was met across all wavelengths, except for 38 anomalous spectral samples, most of which exhibited subpar radiometric performance.

3. RECONSTRUCTION AND CHALLENGES OF AIRS PRE-FLIGHT SPATIAL RESPONSE FUNCTIONS (SPATIALRFS)

The AIRS pre-flight data for the spatial response functions, colloquially referred to as 'tophats' (see Figure 1) consists of two data sets. The first set includes 2D scans across the entire aperture, with each scan representing a weighted average of the A and B sides. The second set comprises 1D scans along the x and y axes for both A and B sides, taken separately. We aim to reconstruct 2D tophats for the A and B sides using these data sets.

Since the measured intensity for each pixel in the 2D tophats is a weighted sum of some A and B intensities, extracting A and B involves apportioning the measured pixel intensity of the 2D tophat to A and B. Several factors complicate the process, including finite size of the measurement beam, misalignment of the 1D and 2D data coordinates, and the non-central positioning of the 1D and 2D data relative to the aperture.

The AIRS tophat data exhibit several deviations from ideal form. These include continuous effects across adjacent detectors such as interference fringes at longer wavelengths, Foreign Object Debris (FOD) on intermediate surfaces, vignetting (mostly at shorter wavelengths), and unusable data due to defective detectors.

The AB reconstruction, described in the next section, involves cleaning up data irregularities and identifying unusable data, subtracting synthetic quadrant tophats, interpolating or scaling the remainders, and apportioning these remainders.

Since the tophats were acquired at the spectrometer level, the impact of the scan mirror, scan motion and post-measurement insertion of a field aperture must be included. These effects are applied to the tophats through analytical means producing a final system SpatialRF, and is discussed below.

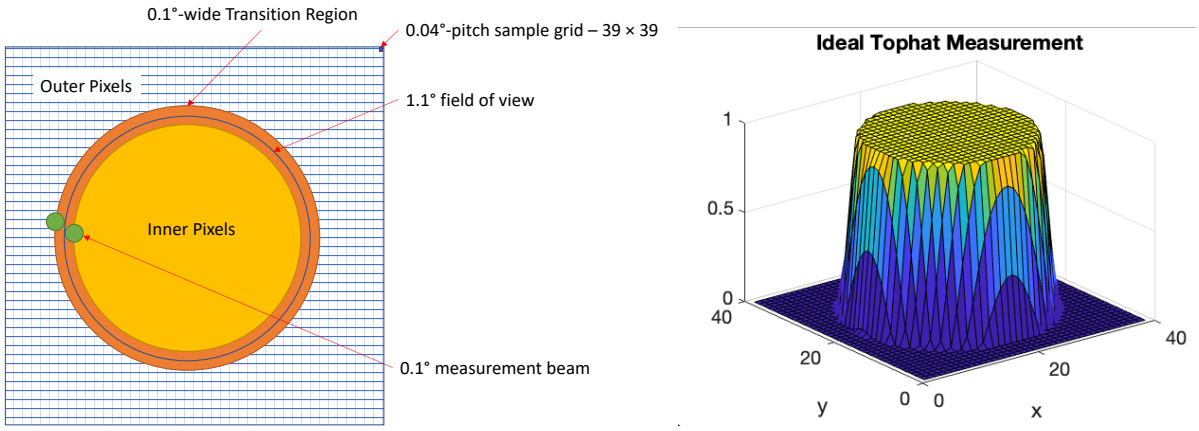

Figure 1. Ideal tophat measurement where the edges are smoothed by the sample to have a width slightly over the Nyquist limit of two pixels. [Left] The blue circle represents the 1.1°-diameter AIRS aperture. The yellow disk is the central flat 'table.' Green disks are 0.1°-diameter example sample beams. The orange torus depicts the edge transition region. [Right] Plot of the analytic calculation.

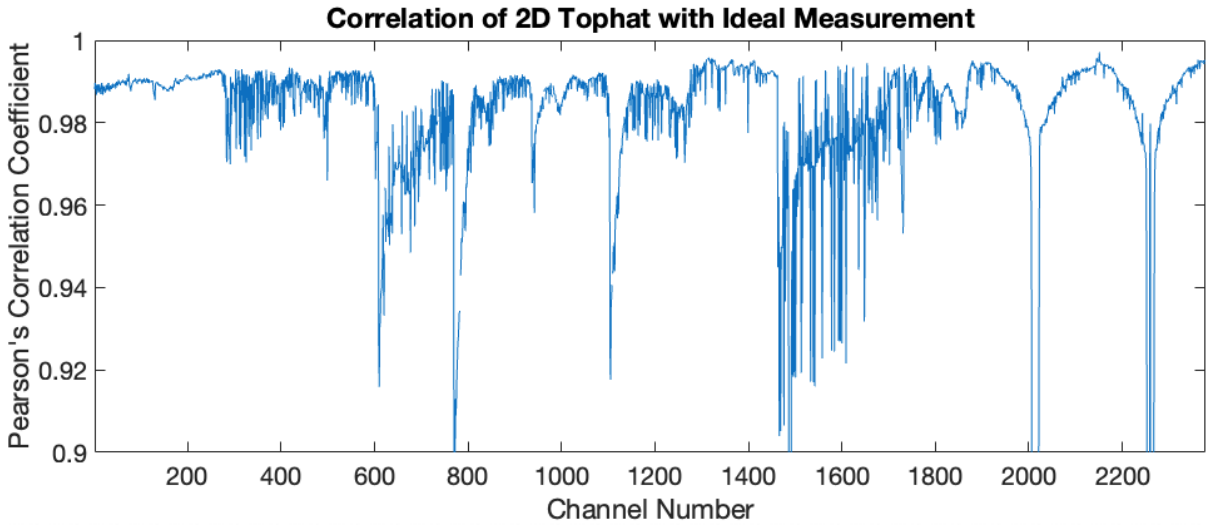

Figure 2. Plot of the correlation between the ideal tophat measurement and the 2D tophat data, with better tophats showing a correlation coefficient near 0.99. The ideal tophat used here was offset by (0.09, -0.04) pixels to maximize the sum of the correlations. However, the sum of all tophat correlations is a very crude measure of fit quality, and subsets of channels receive substantially different offsets. Although we know M8 (channels 609 to 769) is offset, this is barely noticeable in the plot.

4. METHODOLOGY FOR RECONSTRUCTION OF PRE-FLIGHT AIRS SPATIAL RESPONSE FUNCTION MEASUREMENTS

The measurement beam used had a diameter of 0.1°, while the grid spacing was 0.04°, making the measurement beam 2.5 times the grid spacing. This size difference has two major implications: firstly, the sharpness of the aperture edge and other sharp features is degraded; secondly, any sharp feature in the data is likely due to measurement error.

If both the measurement apparatus and the AIRS instrument were "ideal", the resulting tophat measurements would be the convolution of two disks: the disk of the AIRS aperture and the disk of the illuminating test setup beam. Figure 1 illustrates the ideal tophat. The ideal tophat measurement function roughly fits the data (see Figure 2). However, attempts to use the ideal tophat measurement to identify fine details, such as finding coordinate offsets or confirming the sample beam size, were ambiguous at the sub-pixel level. Since the effects

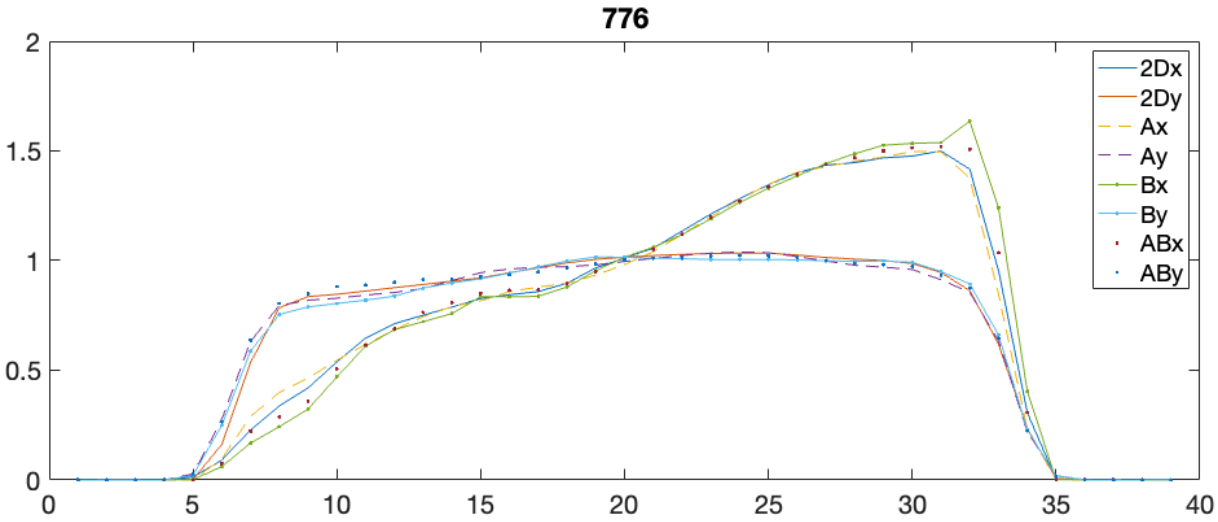

Figure 3. Plot of aligned data for channel 776. '2Dx' and '2Dy' represent the 2D cuts along the x and y symmetry axes of the 2D dataset, respectively. 'Ax', 'Ay', 'Bx', and 'By' denote the 1D scan data. 'ABx' and 'ABy' (dots only) correspond to the equal weights data set.

are small and deconvolution is not possible due to insufficient sampling, the tophat functions are not corrected for the beam size.

Figure 3 shows plots of aligned data for channel 776 ($913.37\,\mathrm{cm}^{-1}$), including 2D cuts along the data set, the 1D scan data, and the equal weights data set. We used 1D data to supplement the computation of the tophat scans for those channels that were missing or dead. Not all channels have A and B sides. The tophat data were taken for a given set of AB SpatialRFs, not A-only and B-only, and our goal was to reconstruct pre-flight tophats for all A and all B. The 1D data for A-only and B-only were used to assist in interpolating for those channels where we did not have A-only and B-only 2D data.

Since we have 1D scans for both A and B sides, roughly along the x- and y-axes, we can use these scans to create a synthetic tophat by interpolating between the axes. The 1D-scan offsets are simple to compensate for along the scans by a simple shift, while cross-scan is relatively complex. The cross-axis scan was rotated to make a two-dimensional function. Figure 4 shows an example where the cross-axis scan data for channel 703 ($881.40\,\mathrm{cm}^{-1}$) are converted into tophats. The interpolation is performed radially over all angles and radii according to:

$$R(r,\theta) = \mathrm{interp}\left\{\left[0,\ \frac{\pi}{2},\ \pi,\ \frac{3\pi}{2},\ 2\pi\right], [L_x(r,0)], [L_y(0,r)], [L_x(-r,0)], [L_y(0,-r)], [L_x(r,0)]\right\}, \qquad (1)$$

where
$R(x,y)$ represents the synthetic tophat function,
$L_{x,y}$ represents the cross-axis scan data.

The radial function is then resampled onto a rectilinear grid corresponding to the 39×39 pixel grid of the measured tophat functions. In some cases, the cross-axis scan data are not usable due to bad detectors or excessive noise. A criterion that requires a Signal-to-Noise Ratio (SNR) of 10:1 is established, where SNR is defined as the mean of pixels in the central 4×4 region of the tophat divided by the standard deviation of the same pixels. If the SNR is less than 10, the tophats are interpolated from adjacent channels that have sufficient SNR. Interpolation is restricted to channels within an AIRS module. In the next step, the difference between the sum of the synthesized tophats, weighted to that of the measured tophats, and the measured tophats themselves are apportioned equally to the A and B sides on a per-pixel basis. This approach ensures that the weighted A and B add up to the 2D tophat data. This process is illustrated in Figure 5 where the AB, A and B tophats

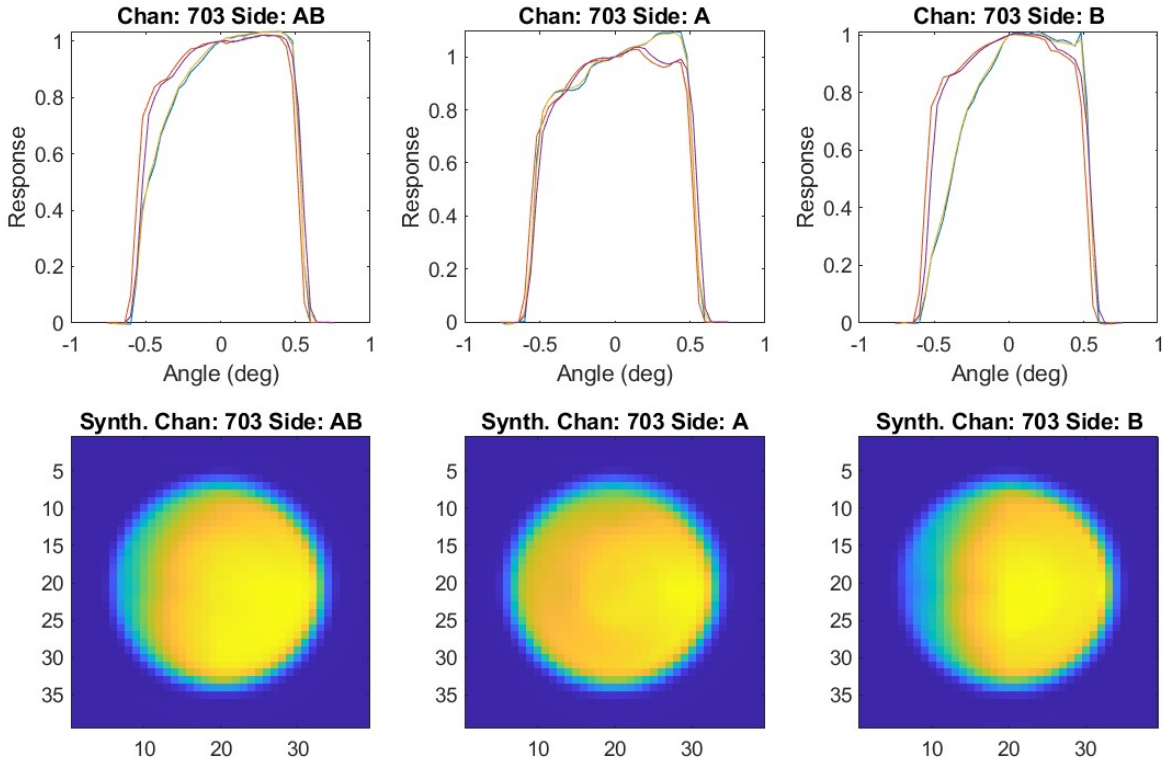

Figure 4. Synthetic tophats generated from cross-axis scan data for AB, A and B sides.

after reapportionment of errors are shown in the top row. Here, slight differences from the cross-axis scan data can be observed. The bottom row compares the summed synthesized tophat to the measured tophat.

The final step in producing an AIRS SpatialRF involves simulating the insertion of the field mask, rotation of the scan mirror, and integration.[10] This simulation begins by cropping the tophat by six pixels on each side to represent the field mask. The image is then rotated using a rotational transform that corresponds to the scan mirror's image rotation, which is equal to the scan angle for each of the 90 footprints. The final step is to convolve the image in the vertical direction with a rectangle function that matches the AIRS integration size of 1.1 degrees. This process, illustrated for channel 703 (881.40 cm^{-1}), is shown in Figure 6. The same above process is performed for all 2378 channels independently for the A, B and AB sides.

SpatialRFs are available in three NetCDF format files: AB_TopHats_v2.A.nc, AB_TopHats_v2.B.nc, and AB_TopHats_v2.AB.nc, corresponding respectively to the A, B, and AB gain settings of the instrument detectors. The Spatial Response Functions are normalized to 1 at the center footprint, located at (20,20) in the 39 x 39 array, and have dimensions (39, 39, 2378, 90). Each file contains the following variables:

Name	Size	Bytes	Class	Comments
AIRS_SpatialRF	39 × 39 × 2378 × 90	1302097680	single	Spatial Response Function for each of AIRS 90 footprints
x_spatial	39 × 39	12168	double	Scan direction angle projected towards Earth relative to the center of AIRS in degrees
y_spatial	39 × 39	12168	double	Track direction angle projected towards Earth relative to the center of AIRS in degrees
wlt	2378 × 1	9512	single	Wavelength (µm)

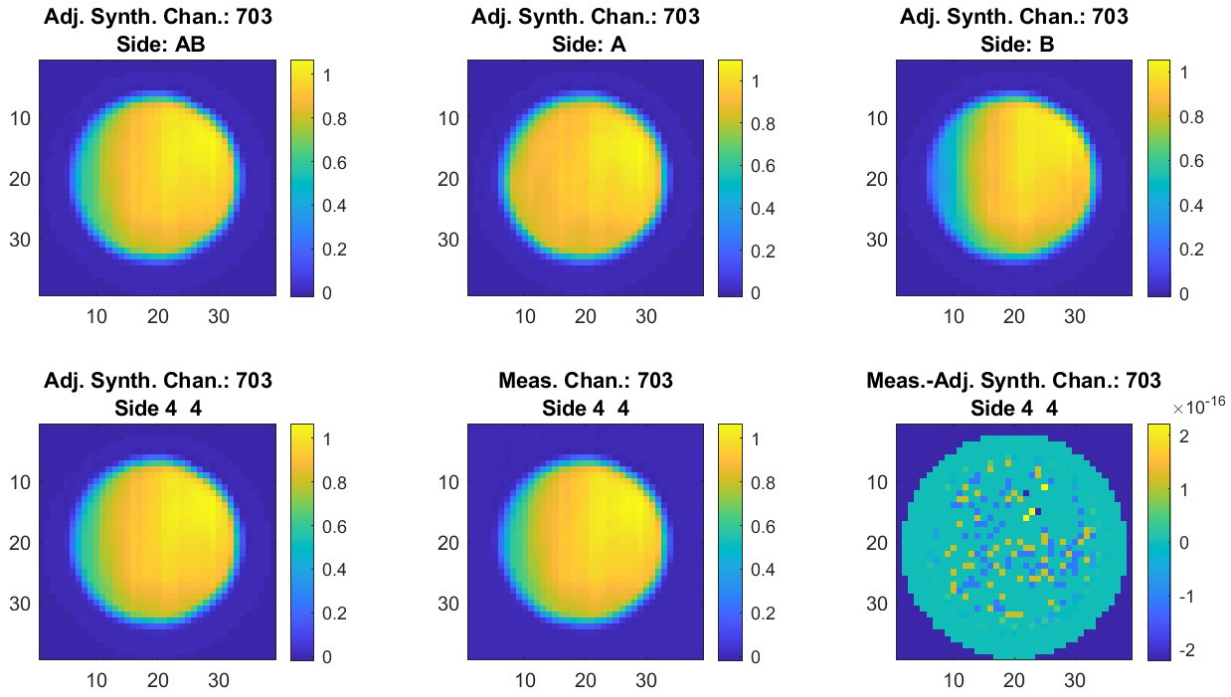

Figure 5. Top row: Synthetic tophats after reapportionment of errors to ensure they match with the measured top hats. Bottom row: Synthetic tophat with as-measured weighting (left), as-measured tophat (center), and difference (right).

The visualizations of SpatialRFs for sides AB, A, and B from these files for channel 703, footprint 45, are depicted in Figure 7 (top row).

5. DERIVING IN-FLIGHT SPATIALRFS FROM AIRS AND MODIS DATA

We assembled the AIRS and MODIS data for comparison, and used the SpatialRF reconstruction model we developed in Ref. 11, 12 to derive in-flight SpatialRFs. The SpatialRFs were derived for consecutive days in March 1, 2003 and March 2, 2003, separately. The channels considered are those that did not change states between pre-flight and in-flight states from March 2003 (i.e. AB→AB, A→A, B→B). The five footprints that were considered are: 1, 22, 45, 68, 90. Only "window" channels that get most of their signal from the surface instead of the atmosphere were used. A simulated clear tropical nadir case was used, with the criterion that the difference between the surface temperature and the calculated brightness temperature is less than 10.0 kelvin, were considered. Higher differences would essentially increase the noise level in our analysis. MODIS Band 31 (886.21 - 927.64 cm^{-1}) was used for these analyses.

We established that AIRS channels (wavenumbers) that are useful to consider with MODIS Band 31 are between 389 (764.20 cm^{-1}) and 1396 (1299.70 cm^{-1}).

We determined that there are 176 channels that satisfy our criteria, and they range from channel 389 to 1264, with corresponding wavenumbers ranging from 764.2 cm^{-1} and 1217.5 cm^{-1}. With 176 channels, 5 footprints per channels, and two separate days considered, there were a total of 1760 SpatialRFs reconstructed.

Figure 7 (middle row) depicts the in-flight SpatialRFs for channel 703, footprint 45, on March 1, 2003 (Day 1) and March 2, 2003 (Day 2), as well as the difference between the SpatialRFs for Day 1 and Day 2. Both pre-flight and in-flight states from March 2003 were at AB for this channel. Figure 7 (bottom row) shows the difference between the in-flight SpatialRF for Day 1 and the pre-flight SpatialRF for side AB.

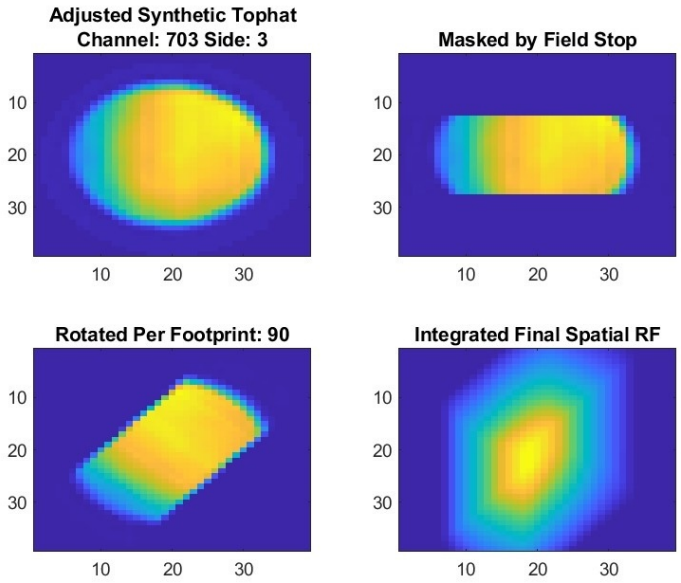

Figure 6. Formation of the Spatial Response Function for the B side of channel 703. Top Left: Tophat distribution measured pre-flight. Top Right: Tophat cropped commensurate with the insertion of a field mask post-measurement. Bottom Left: Tophat rotated for footprint 90. Bottom Right: Spatial Response Function computed after integrating the tophat function, commensurate with the motion of the truncated tophat due to scanning.

6. QUANTIFYING UNCERTAINTIES IN SPATIAL RESPONSE FUNCTIONS

We use the total variation distance metric to quantify the difference between two SpatialRFs. The total variation distance between two spatial response functions, F_1 and F_2, over a domain Ω is defined as:

$$TV(F_1, F_2) = \frac{1}{2} \sum_{(x,y)\in\Omega} |F_1(x,y) - F_2(x,y)|.$$

This metric sums the absolute differences between the normalized SpatialRFs and then halves the result. It ranges from 0 to 1, where 0 indicates that the two distributions are identical (0% difference), and 1 indicates that they are completely different (100% difference). This metric can be used to compare how similar or different two SpatialRFs are.

To determine uncertainties in retrieved *in-flight* SpatialRFs, a total variation distance metric between SpatialRFs generated from two consecutive days is considered, namely $TV(F_{\text{Day 1}}, F_{\text{Day 2}})$. To determine uncertainties in *pre-flight* SpatialRFs, a difference metric between a retrieved in-flight SpatialRF and a processed pre-flight SpatialRF is used, namely $TV(F_{\text{Day 1}}, F_{\text{pre-flight}})$. The effective uncertainty of a pre-flight SpatialRF, relative to retrieved $F_{\text{Day 1}}$ and $F_{\text{Day 2}}$, would be the additional uncertainty beyond the baseline level of uncertainty between $F_{\text{Day 1}}$ and $F_{\text{Day 2}}$. This is calculated as:

$$\text{Effective Uncertainty of } F_{\text{pre-flight}} = TV(F_{\text{Day 1}}, F_{\text{pre-flight}}) - TV(F_{\text{Day 1}}, F_{\text{Day 2}}).$$

The effective uncertainty of a pre-flight SpatialRF indicates additional uncertainty beyond the normal day-to-day variability or noise level observed between $F_{\text{Day 1}}$ and $F_{\text{Day 2}}$.

7. RESULTS OF UNCERTAINTY ANALYSIS IN AIRS SPATIAL RESPONSE FUNCTIONS

We quantified uncertainties in AIRS pre-flight SpatialRFs and retrieved in-flight SpatialRFs for 176 channels, each for five different scan angles. We first normalized SpatialRFs such that their sums equal 1. As a result, their difference is essentially a difference in distribution or shape.

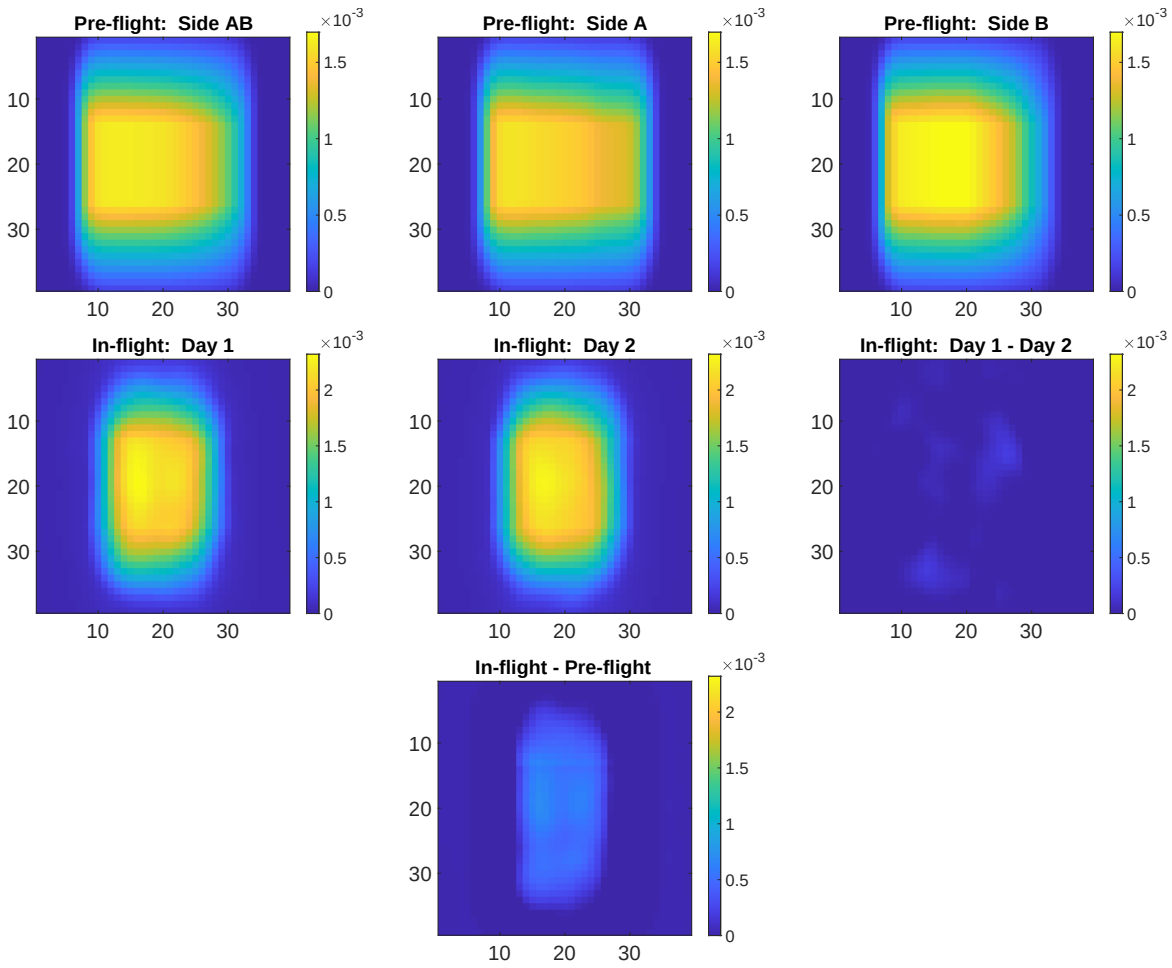

Figure 7. SpatialRFs for Channel 703, Footprint 45. Top row: Pre-flight SpatialRFs for sides AB, A, and B. Middle row: In-flight SpatialRFs for March 1, 2003 (Day 1), March 2, 2003 (Day 2), and the difference between SpatialRFs for Day 1 and Day 2. Bottom row: Difference between the in-flight SpatialRF for Day 1 and the pre-flight SpatialRF for side AB.

Figure 8 displays plots of uncertainties in AIRS retrieved in-flight SpatialRFs (top) and effective uncertainties in AIRS pre-flight SpatialRFs (bottom). These uncertainties are expressed as percentages and plotted against the channel for five different scan angles. The mean uncertainties for retrieved in-flight SpatialRFs across all channels are 5.73%, 5.34%, 4.98%, 4.84%, and 6.16% for Footprints 1, 22, 45, 68, and 90, respectively, with an overall mean of 5.41%. Similarly, the mean effective uncertainties for pre-flight SpatialRFs are 17.08%, 13.49%, 19.84%, 14.25%, and 14.95%, for the same footprints, with an overall mean of 15.92%.

For channel 703, footprint 45, as depicted in Figure 7, the uncertainty in the retrieved in-flight SpatialRF is 2.27%. The corresponding effective uncertainty in the pre-flight SpatialRF is 22.32%.

ACKNOWLEDGMENTS

This work was conducted at the Jet Propulsion Laboratory, California Institute of Technology, under a contract with the National Aeronautics and Space Administration (80NM0018D0004).

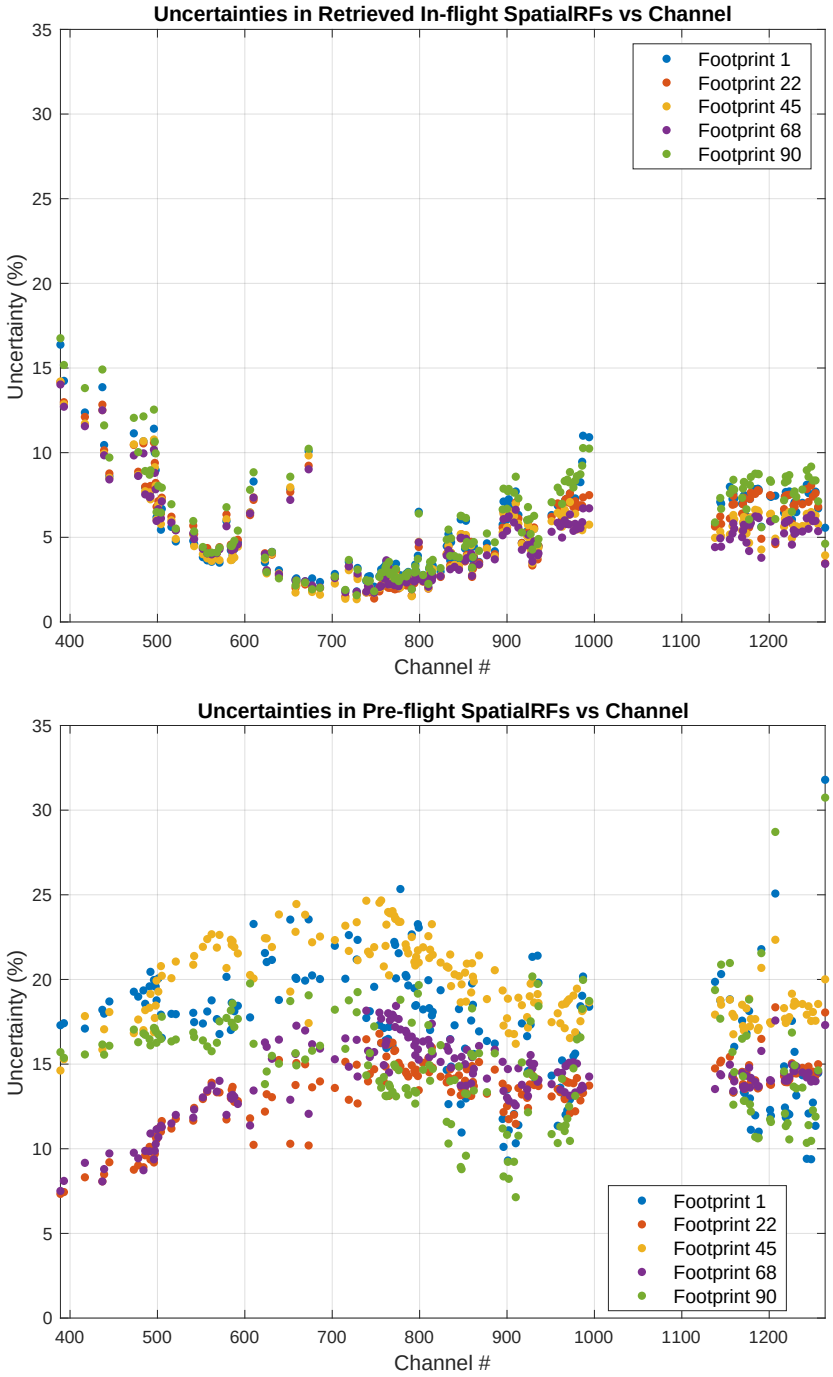

Figure 8. Plot of uncertainties in AIRS retrieved in-flight SpatialRFs (top) and pre-flight SpatialRFs (bottom), expressed as percentages, versus channel for five different footprints.

REFERENCES

[1] Susskind, J., Blaisdell, J., and Iredell, L., "Improved methodology for surface and atmospheric soundings, error estimates, and quality control procedures: The AIRS science team version-6 retrieval algorithm," *J. Appl. Remote Sens.* **8**(1), 084994 (2014).

[2] Zheng, J., Li, J., Schmit, T. J., Li, J., and Liu, Z., "The impact of AIRS atmospheric temperature and mois-

ture profiles on hurricane forecasts: Ike (2008) and Irene (2011)," *Advances in Atmospheric Sciences* **32**(3), 319–335 (2015).

[3] Boullot, N., Rabier, F., Langland, R., Gelaro, R., Cardinali, C., Guidard, V., Bauer, P., and Doerenbecher, A., "Observation impact over the southern polar area during the Concordiasi field campaign," *Quarterly Journal of the Royal Meteorological Society* **142**, 597–610 (2016).

[4] Pagano, T. S., Chahine, M. T., and Fetzer, E. J., "The Atmospheric Infrared Sounder (AIRS) on the NASA Aqua Spacecraft: a general remote sensing tool for understanding atmospheric structure, dynamics, and composition," in [*Remote Sensing of Clouds and the Atmosphere XV*], Picard, R. H., Schäfer, K., Comeron, A., and van Weele, M., eds., **7827**, 78270B, International Society for Optics and Photonics, SPIE (2010).

[5] Pierce, D., Barnett, T., Fetzer, E., and Gleckler, P., "Three-dimensional tropospheric water vapor in coupled climate models compared with observations from the AIRS satellite system," *Geophysical Research Letters* **332**, L21701 (2006).

[6] Dessler, A., Zhang, Z., and Yang, P., "Water-vapor climate feedback inferred from climate fluctuations, 2003-2008," *Geophysical Research Letters* **35**, L20704 (2008).

[7] Barnes, W. L., Pagano, T. S., and Salomonson, V. V., "Prelaunch characteristics of the Moderate Resolution Imaging Spectroradiometer (MODIS) on EOS-AM1," *IEEE Transactions on Geoscience and Remote Sensing* **36**(4), 1088–1100 (1998).

[8] Pagano, T. S., Aumann, H. H., Manning, E. M., Elliott, D. A., and Broberg, S. E., "Improving AIRS radiance spectra in high contrast scenes using MODIS," in [*Earth Observing Systems XX*], Butler, J. J., Xiong, X. J., and Gu, X., eds., **9607**, 96070K, International Society for Optics and Photonics, SPIE (2015).

[9] Overoye, K., Aumann, H. H., Weiler, M. H., Gigioli, G. W., Shaw, W., Frost, E., and McKay, T., "Test and calibration of the AIRS instrument," in [*Infrared Spaceborne Remote Sensing VII*], Strojnik, M. and Andresen, B. F., eds., **3759**, 254 – 265, International Society for Optics and Photonics, SPIE (1999).

[10] Elliott, D. A., Pagano, T. S., and Aumann, H. H., "The impact of the AIRS spatial response on channel-to-channel and multi-instrument data analyses," in [*Earth Observing Systems XI*], Butler, J. J., ed., **6296**, 62960I, International Society for Optics and Photonics, SPIE (2006).

[11] Yanovsky, I., Pagano, T. S., Manning, E. M., Broberg, S. E., Aumann, H. H., and Vese, L. A., "AIRS point spread function reconstruction using AIRS and MODIS data," in [*2021 IEEE International Geoscience and Remote Sensing Symposium IGARSS*], 7868–7871 (2021).

[12] Yanovsky, I., Pagano, T. S., Manning, E. M., Broberg, S. E., Aumann, H. H., and Vese, L. A., "Learning spatial response functions from large multi-sensor AIRS and MODIS datasets," in [*Earth Observing Systems XXVI*], Butler, J. J., Xiong, X. J., and Gu, X., eds., **11829**, 118290A, International Society for Optics and Photonics, SPIE (2021).